Bioorganic & Medicinal Chemistry 25 (2017) 2378–2386

Contents lists available at ScienceDirect

Bioorganic & Medicinal Chemistry

journal homepage: www.elsevier.com/locate/bmc

Synthesis, properties, antitumor and antibacterial activity of new Pt(II) and Pd(II) complexes with 2,2′-dithiobis(benzothiazole) ligand

Simona Rubino *, Rosalia Busà, Alessandro Attanzio, Rosa Alduina, Vita Di Stefano, Maria Assunta Girasolo, Santino Orecchio, Luisa Tesoriere

Dipartimento di Scienze e Tecnologie Biologiche, Chimiche e Farmaceutiche (STEBICEF), Università di Palermo, Viale delle Scienze pad. 16, Parco d'Orleans, 90128 Palermo, Italy

ARTICLE INFO

Article history:
Received 15 December 2016
Revised 23 February 2017
Accepted 24 February 2017
Available online 9 March 2017

Keywords:
Platinum complex
Palladium complex
Heterocyclic nitrogen ligand
Anticancer activity
Antimicrobial activity

ABSTRACT

Mono- and binuclear Pt(II) and Pd(II) complexes with 2,2′-dithiobis(benzothiazole) (DTBTA) ligand are reported. [Pt(DTBTA)(DMSO)Cl]Cl·$CHCl_3$ (**1**) and $[Pd_2(\mu\text{-}Cl)_2(DTBTA)_2]Cl_2$ (**2**) have been synthesized and structurally characterized by elemental analysis, IR, ^1H and ^{13}C NMR spectroscopy, MS spectrometry and the content of platinum and palladium was determined using a flame atomic spectrometer. Two different coordination modes of **1** and **2** complexes were found; in both complexes, the coordination of Pt(II) and Pd(II) ions involves the N(3) atoms of the ligand but the binuclear complex **2**, is a *cis*-chloro-bridged palladium complex. Evaluation of their in vitro antitumor activity against two human tumor cell lines human breast cancer (MCF-7) and hepatocellular carcinoma (HepG2); and their antimicrobial activity against *Escherichia coli* and *Kokuria rhizophila* was performed. Only complex **1** showed a dose- and time-dependent cytotoxic activity against the two tumor cell lines, associated to apoptosis and accumulation of treated cells in G0/G1 phase of cell cycle, while both **1** and **2** exhibited antimicrobial activity with complex **1** much more potent. The study on intracellular uptake in both MCF-7 and HepG2 cell lines revealed that only platinum of complex **1** is present inside the cells, suggesting a different mode of action of the two compounds. This was also in agreement with the results obtained for the antitumor and antibacterial activity.

1. Introduction

The development of new antimicrobial and anticancer therapeutic agents is one of the fundamental goals in medicinal chemistry. In this field the chemistry of heterocyclic compounds and of their complexes with Pt(II) and Pd(II) metallic ions is one of the leading lines of investigations in both inorganic and organic chemistry. There are vast numbers of pharmacologically active heterocyclic compounds, many of which are regularly in clinical use.

Five membered heterocyclic compounds containing Nitrogen, Sulphur and Oxygen have occupied enormous significance in the field of drug discovery process.[1] Among pharmacologically important heterocyclic compounds, the Benzothiazole (BTA) and its derivatives are the most important heterocyclic compounds, which are common and integral feature of natural products and pharmaceutical agents and show a variety of pharmacological properties. BTA analogs offer a high degree of structural diversity that has proven to be useful for the search of new therapeutic agents that exert a wide range of biological activities such as anticancer, antimicrobial, anticonvulsant, antiviral, antitubercular, antimalarial, anthelmintic, analgesic, anti-inflammatory, antidiabetic and fungicidal activity.[2] The BTA is a heterocyclic compound in which benzene ring is fused to 4,5-positions of thiazole ring, is completely planar, and is potentially ambidentate with N and S available to coordination when it is used as ligand in metal ion complexes. The thiazole core is present in many biologically relevant molecules, which are in therapeutic use, such as Sulfathiazole (antimicrobial drug), Ritonavir (antiretroviral drug), Abafungin (antifungal drug), Tiazofurin (antineoplastic agent), Meloxicam

Abbreviations: AO, Acridine Orange; BTA, Benzothiazole; DTBTA, 2,2′-dithiobis (benzothiazole); DTT, 1, 4-Dithiothreitol; DMF, dimethylformamide; DMSO, dimethylsulfoxide; EB, Ethidium Bromide; EDTA, Ethylenediaminetetraacetic acid; FACS, Fluorescence-Activated Cell Sorting; FBS, Fetal Bovine Serum; FITC, Fluorescein isothiocyanate; MS, Mass Spectrometry; HESI, Heated Electrospray Ionization; MIC, Minimal inhibitory concentration; MTT, 3-(4,5-dimethyl-2-thiazolyl)bromide-2,5-diphenyl-2H-tetrazolium; PBS, phosphate buffer; PI, Propidium Iodide; PS, phosphatidylserine; RPMI, Roswell Park Memorial Institute; TBE, Tris/Borate/EDTA; TLC, Thin Layer Chromatography; TMS, tetramethylsilane.

* Corresponding author. Tel.: +39-091-23897972; fax: +39-091-6577270.
E-mail address: simona.rubino@unipa.it (S. Rubino).

http://dx.doi.org/10.1016/j.bmc.2017.02.067
0968-0896/

(non-steroidal anti-inflammatory drug), Nitazoxanide (antiprotozoal agent).[3] They contain extended *p*-delocalized systems which are capable of binding to DNA molecules via *p*–*p* interactions. In this paper, our scope was to design new molecules for improvement of the use of Pt compounds in chemotherapy, reducing toxicity, increasing clinical effectiveness, broader spectrum of action, elimination of side effects and increasing solubility. Using benzothiazole scaffold and synthetic procedure followed by suitable modification to generate diversified compounds, new complexes for antimicrobial and anticancer activity were designed.[4] Platinum(II) and palladium(II) ions have similar chemical properties and modes of coordination forming square planer complexes[5]; in fact, they both adopt dsp^3 orbital hybridization[6], but the palladium compounds are more labile from both a thermodynamic and a kinetic point of view with respect to corresponding platinum compounds. Palladium-based drugs can undergo a rapid hydrolysis before they reach the DNA target; this results in both a low antitumor activity or even inactivity and toxicity.[7] The use of bulkier chelating ligands can make them active against tumor.[8] For this reason we have chosen to synthesize and characterize with elemental analysis, IR and ^{1}H and ^{13}C NMR spectroscopy, MS spectrometry, new mononuclear platinum(II) [Pt(DTBTA)(DMSO)Cl]Cl·$CHCl_3$ (**1**) and binuclear bridged palladium(II) [$Pd_2(\mu\text{-}Cl)_2(DTBTA)_2$]$Cl_2$ (**2**) complexes with a derivate of benzothiazole, 2,2′-dithiobis(benzothiazole) (DTBTA) ligand and to study their biological activity. Our research group has experience in the synthesis and biological study of mono- and polynuclear Pt(II) complexes[9–11], so we decided to investigate the antitumor activity of **1** and **2** in vitro against two human cell lines HepG2 and MCF-7. The antimicrobial activity against *Escherichia coli* and *Kokuria rhizophila* of these compounds is also reported.

2. Materials and methods

2.1. General experimental conditions

Dipotassium tetrachloroplatinum(II), dipotassium tetrachloropalladium(II), dimethyl sulfoxide and 2,2′-dithiobis(benzothiazole) (DTBTA) were purchased from Aldrich (Milan, Italy). The products were used without further purification. Syntheses were performed with exclusion of moisture and direct light.

Owing to poor aqueous solubility, the tested complexes, for biological studies, were dissolved in DMSO and then diluted in culture medium so that the effective DMSO concentration did not exceed 0.1%. Cell lines of MCF-7 (human breast cancer) and HepG2 (human hepatocellular carcinoma) were purchased from American Type Culture Collection, Rockville, MD, USA. Elemental analysis for C, H, N, S, were performed at the Laboratory of Microanalysis (University of Padova, Italy), chlorine was determined by potentiometric titration with standard silver nitrate after combustion in pure oxygen according to Schöninger.[12] The IR spectra were recorded, as Nujol mulls, with a FT-IR Bruker Vertex 70 Advanced Research. Conductivity measurements for 10^{-3} M solutions in DMSO were obtained with a Crison GLP 31 Model Conductometer. The determination of platinum and palladium contents was obtained using a flame atomic spectrometer Perkin-Elmer 372 and the average of four independent measurements was determined. ^{1}H and ^{13}C NMR spectra were measured in DMSO-d_6 at 300.13 and 75.47 MHz respectively, using a Bruker AC series 300 MHz spectrometer (TMS as an internal standard): chemical shifts are expressed in δ values (ppm). Mass Spectrometry (MS) spectra were determined with Q-Exactive High Resolution mass spectrometer (Thermo Scientific, Germany) equipped with the HESI electrospray source. The experiments were performed in positive ion mode at a resolving power of 17,500 FWHM (at *m*/*z* 200). Samples prepared in 50/50 aqueous/MeOH (20 μL) were introduced into the mass spectrometer by flow infusion using a head pressure of 35–45 psi at approximately 50 μL/min via the ESI-chip. To evaluate the cellular uptake, the complexes **1** and **2** were calcined at 600 °C in a muffle and the residues were dissolved in solution of HNO_3/HCl (1:3). They were analyzed with Differential Pulse Voltammetry Amel 433 to calculate the ng/cell of intracellular metals.

2.2. Chemistry

A general procedure for the synthesis of the complexes **1** and **2** was adopted. The complex **1** was synthesized by *Cis*-[$Pt(DMSO)_2Cl_2$][13] (0.33 g, 1 mmol) that was added solid to the chloroform solution (25 ml) of the DTBTA (0.421 g, 1 mmol); for the complex **2** an aqueous solution of K_2PdCl_4 (0.26 g, 1 mmol) was added dropwise in stirring to the ligand solution (0.27 g, 1 mmol) in ethanol (30 ml). The resulting solutions were stirred for 24 h at 40 °C for complex **1** and 70 °C for complex **2**. The orange solids were filtered, washed with chloroform and dried *in vacuum* over P_4O_{10}.

2.2.1. [Pt(DTBTA)(DMSO)Cl]Cl·$CHCl_3$ (**1**)

The complex **1** was prepared following the general procedure. Yield 40%. *Anal.* Calc. for ($C_{16}H_{14}N_2OS_5PtCl_2$)·$CHCl_3$ (795.99): C, 25.65; H, 1.90; N, 3.52; S, 20.14; Cl, 22.27; Pt, 24.51%. Found: C, 25.83; H, 1.61; N, 3.63; S, 20.54; Cl, 22.67; Pt, 24.12. Melting point: >350 °C. Conductivity measurements of the complex for 10^{-3} M solution in DMSO afforded a value Λ_M = 31.02 Ω^{-1} cm^2 mol^{-1} [14] IR (cm^{-1}) for the ligand: 1559 *ν*(C=N), 1156 *ν*(C–N), 1006 *ν*(C–S) and for the complex 1541 *ν*(C=N), 1157 *ν*(C–N), 1006 *ν*(C–S), 1132 *ν*(S=O of coord. DMSO), 349 *ν*(Pt–Cl), 379 *ν*(Pt–S) and 285 *ν*(Pt–N). ^{1}H NMR for the ligand (DMSO-d_6, 300 MHz) δ ppm: 8.07 (d, 2H, $C_4HC_{4'}H$), 7.95 (t, 2H, $C_5HC_{5'}H$), 7.53 (d, 2H, $C_7HC_{7'}H$), 7.44 (t, 2H, $C_6HC_{6'}H$); for the complex (DMSO-d_6, 300 MHz) δ ppm: 9.07 (d, 2H, $C_4HC_{4'}H$), 8.29 (t, 2H, $C_5HC_{5'}H$), 7.84 (d, 2H, $C_7HC_{7'}H$), 7.68 (t, 2H, $C_6HC_{6'}H$), 7.26 (s, 1H, $CHCl_3$), 3.67 (s, 6H, coord. DMSO); $^3J_{C4HC5H}$ = 8.1; Hz; $^3J_{C5HC6H}$ = 7.8 Hz; $^3J_{C6HC7H}$ = 8.1 Hz. ^{13}C NMR (DMSO-d_6, 75 MHz) δ ppm for the ligand: 148.00 (C_2), 126.78 (C_8, C_9), 125.35(C_4,C_7), 122.21 (C_5,C_6); for complex: 155.94 (C_2), 153.00 ($C_{2'}$), 131.09 (C_8), 127.35 ($C_{8'}$), 127.16 (C_9), 127.01($C_{9'}$), 126.16 (C_4), 126.11 ($C_{4'}$), 123.60 (C_7), 123.17 ($C_{7'}$), 122.91 (C_5,$C_{5'}$), 122.40 (C_6,$C_{6'}$), 23.25 ($CHCl_3$), 14.16 (DMSO). ESI(+)-MS: $[M]^+$ $C_{16}H_{14}N_2OS_5PtCl$: 639.399 a.m.u.; $[M]^{2+}$ $C_{16}H_{14}N_2OS_5Pt$: 302.306.

2.2.2. [$Pd_2(\mu\text{-}Cl)_2(DTBTA)_2$]$Cl_2$ (**2**)

The complex **2** was prepared following the general procedure. Yield 60%. *Anal.* Calc. for $C_{28}H_{16}N_4S_8Pd_2Cl_4$ (1019.64): C, 32.98; H, 1.58; N, 5.49; S, 25.16; Cl, 13.91; Pd, 20.87%. Found: C, 33.05; H, 1.90; N, 5.75; S, 24.80; Cl, 13.67; Pd, 21.05. Melting point: >350 °C. Conductivity measurements of the complex for 10^{-3} M solution in DMSO afforded a value Λ_M = 34.4 Ω^{-1} cm^2 mol^{-1} [14]. IR (cm^{-1}) for the complex 1564 *ν*(C=N), 1156 *ν*(C–N), 1005 *ν*(C–S), 393 *ν*(Pd–Cl), and 258 *ν*(Pd–N). ^{1}H NMR for the complex (DMSO-d_6, 300 MHz) δ ppm: 9.11 (d, 4H, $C_4HC_{4'}H$), 9.09 (d, 4H, $C_7HC_{7'}H$), 7.70 (dd, 4H, $C_5HC_{5'}H$), 7.47 (dd, 4H, $C_6HC_{6'}H$). ^{13}C NMR (DMSO-d_6, 75 MHz) δ ppm for the complex: 132.00 (C_4,$_{4'}$), 128.00 (C_7,$_{7'}$), 124.00 ($C_{5,5'}$), 126.00 ($C_{6,6'}$). $^3J_{C4HC5H}$ = 8.1 Hz; $^3J_{C5HC6H}$ = 8.1 - Hz; $^3J_{C6HC7H}$ = 8.1 Hz. ESI(+)-MS: $[M]^{2+}C_{28}H_{16}N_4S_8Pd_2Cl_2$: 473.838 *m*/*z*.

2.3. Antimicrobial activity

The antimicrobial activity of the complexes **1** and **2** was determined using the paper disc plate method as previously described[15,16] using Luria Bertani broth agar medium (LB-agar; 10 g/l Tryptone, 5 g/l yeast extract, 10 g/l NaCl, 18 g/l Bacto agar,

pH = 7–7.2). LB agar is a rich medium for microbial growth. The antimicrobial activities were initially investigated using *Kokuria rhizophila* (previously *Micrococcus luteus*) ATCC9341[17] and *Escherichia coli* DH10B as models for Gram-positive and Gram-negative bacteria, respectively. Thus, antimicrobial activity was also tested against a collection of pathogenic bacteria, such as toxigenic isolates of *Staphylococcus aureus*.[18] Briefly, a dense suspension of each microorganism was prepared with a count of approximately 10^8 cells/ml. A 100 μl of microbial suspension was spread onto LB-agar plates. Each of the compounds was dissolved in DMSO and solutions of the complexes at different concentrations were prepared separately. Paper discs of Whatman filter paper (No. 42) of uniform diameter (6 mm) were cut and sterilized in an autoclave. Different amounts of complex **1** or complex **2** were directly spotted on sterile paper discs that were placed on the overlay of bacteria on agar plate in the dark. Growth inhibition halos were observed after overnight incubation at 37 °C. Minimal inhibitory concentration (MIC) was deduced considering as the lowest concentration of the compound still able to produce a transparent halo of growth inhibition larger than 6 mm (size of the disk paper) in a plate containing 20 ml of LB-agar. The antimicrobial activity was calculated at least as a mean of three replicates. Antimicrobial activities of complexes **1** and **2** were compared to tetracycline, cisplatin and the ligand 2,2′-dithiobis(benzothiazole) (DTBTA).

2.4. DNA binding activity using gel electrophoresis

For the gel electrophoresis experiments, the method reported in[19] was carried out: different amounts of the complexes were added to 100 ng of pUC19 DNA in a buffer containing 12.5 mM Tris-HCl pH = 7.5, 10% glycerol, 62.5 mM KCl, 0.75 mM DTT in a final volume of 20 μl and incubated for 30 min at room temperature. 1% agarose gel was prepared in 0.5× TBE buffer (5× TBE: 54 g Tris Base, 27.5 g boric acid, 20 ml of EDTA 0.5 pH = 8). Then 10 μl each of the incubated complex-DNA mixtures (mixed with bromophenol blue dye at a 1:1 ratio) was loaded on the gel containing EtBr (ethidium bromide) along with the pUC19 DNA as reference, and the electrophoresis was carried out under 0.5X TBE buffer system on the dark. At the end of the electrophoresis, the gel was visualized under UV light using a Bio-Rad Trans illuminator. The illuminated gel was photographed by using a Polaroid camera.

2.5. Viability assay in vitro

HepG2 and MCF-7 cell lines were grown in RPMI medium supplemented with l-glutamine (2 mM), 10% fetal bovine serum (FBS), penicillin (100 U/ml), streptomycin (100 μg/ml) and gentamicin (5 μg/ml). HepG2 culture medium also contained sodium pyruvate (1.0 mM). Cells were maintained in log phase by seeding twice a week at a density of 3×10^8 cells/L in humidified 5% CO_2 atmosphere, at 37 °C. In all experiments, after plating, cells were allowed to adhere overnight and then treated with the compounds or vehicle alone (control cells). No differences were found between cells treated with DMSO 0.1% and untreated cells in terms of cell number and viability.

Cytotoxic activity of the complexes **1** and **2** against human tumor cell lines was determined by the MTT colorimetric assay based on the reduction of 3-(4,5-dimethyl-2-thiazolyl)bromide-2,5-diphenyl-2H-tetrazolium (MTT) to purple formazan by mitochondrial dehydrogenases of living cells. This method is commonly used to illustrate inhibition of cellular proliferation. Monolayer cultures were treated for 24–72 h with various concentrations (0.1–100 μM) of the drugs. Cisplatin and ligand were used for comparison. Briefly, all cell lines were seeded at 2×10^4 cells/well in 96-well plates containing 200 μL RPMI. When appropriated, cells were washed with fresh medium and incubated with the compounds in RPMI. After a 24–72 h incubation, cells were washed, and 50 μl FBS-free medium containing 5 mg/ml MTT were added. The medium was discarded after 2 h incubation at 37 °C by centrifugation, and formazan blue formed in the cells was dissolved in DMSO. The absorbance, measured at 570 nm in a microplate reader (Bio-RAD, Hercules, CA), of MTT formazan of control cells was taken as 100% of viability. IC_{50} value for each assessed compound was calculated by plotting the percentage viability versus concentration and reading off the concentration at which 50% of cells remained viable relative to the control. Each experiment was repeated at least three times in triplicate to obtain the mean values.

2.6. Measurement of phosphatidylserine exposure

The externalization of phosphatidylserine (PS) to the cell surface was detected by flow cytometry by double staining with Annexin V-Fluorescein isothiocyanate (Annexin V-FITC)/propidium iodide (PI). Phosphatidylserine, which is normally located on the cytoplasmic surface of cell membranes, is exposed on the cell surface upon induction of apoptosis. Annexin V binds to phosphatidylserine and is used to identify the earliest stage of apoptosis. PI, which does not enter cells with intact membranes, is used to distinguish between early apoptotic cells (Annexin V-FITC positive and PI negative) and late apoptotic cells (Annexin V-FITC/PI-double positive). Tumor cells (HepG2, MCF-7) were seeded in triplicate in 24-wells culture plates at a density of 5.0×10^4 cells/cm^2. After an overnight incubation, the cells were washed with fresh medium and incubated with the compounds in RPMI. After 24 h, cells were harvested by trypsinization and adjusted at 1.0×10^6 cells/ml with buffer according to the manufacturer' instructions (eBioscience, San Diego, CA). One hundred μl of cell suspended solution was added to a new tube, and incubated with Annexin V-FITC and PI solution at room temperature in the dark for 15 min. Then samples of at least 1.0×10^4 cells were subjected to fluorescence-activated cell sorting (FACS) analysis by Epics XL™ flow cytometer using Expo32 software (Beckman Coulter, Fullerton, CA), using appropriate 2-bidimensional gating method.

2.7. Cell cycle analysis

Cell cycle stage was analyzed by flow cytometry. Aliquots of $1x10^6$ cells were harvested by centrifugation, washed with PBS and incubated in the dark in a PBS solution containing 20 μg/ml propidium iodide (PI) and 200 μg/ml RNase, for 30 min, at room temperature. Then samples were immediately subjected to FACS analysis. At least 1×10^4 cells were analyzed for each sample.

2.8. Acridine orange and Ethidium bromide morphological fluorescence dye staining

Acridine orange (AO) stains DNA bright green, allowing visualization of the nuclear chromatin pattern and stains both live and dead cells. Ethidium bromide (EB) stains DNA orange but is excluded by viable cells. Dual staining allows separate enumeration of populations of viable non apoptotic, viable (early) apoptotic, nonviable (late) apoptotic, and necrotic cells. Live cells appear uniformly green. Early apoptotic cells stain green and contain bright green dots in the nuclei as a consequence of chromatin condensation and nuclear fragmentation. Late apoptotic cells incorporate EB and therefore stain orange, but, in contrast to necrotic cells, the late apoptotic cells show condensed and often fragmented nuclei. Necrotic cells stain orange, but have a nuclear morphology resembling that of viable cells, with no condensed chromatin. Briefly,

after tumor cells (HepG2, MCF-7) were treated with the complexes **1** and **2** for 24 h, the medium was discarded. Cells were washed with saline 5 mM phosphate buffer (PBS) and then incubated with 100 µl PBS containing 100 µg/ml of EB plus 100 µg/ml of AO. After 20 min, EB/AO solution was discarded and cells immediately visualized by means of fluorescent microscope equipped with an automatic photomicrograph system (Leica, Wetzlar, Germany). Multiple photos were taken at randomly selected areas of the well to ensure that the data obtained are representative.

2.9. In vitro cellular uptake

For platinum and palladium cellular uptake studies, MCF-7 and HepG2 cells were incubated with the compounds at 25 µM or 100 µM concentration respectively. After 24 h the cells were washed three times with cold PBS (Phosphate Buffered Saline), collected by trypsinization and centrifuged at 1000*g* for 5 min. At the end the pellet was suspended in Milli-Q water, sonicated and the platinum and palladium contents measured with Differential Pulse Voltammetry Amel 433. Instrumental settings were optimized in order to yield maximum sensitivity for platinum and palladium. The data were expressed as ng/cell of Pt or Pd, and were the results of three independent experiments ± SD.

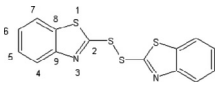

Scheme 1. Structure of the ligand and numbering scheme of atoms.

3. Results and discussion

3.1. Chemistry

The coordination mode of the complexes was determined by using the ^{1}H and ^{13}C NMR and IR spectra. NMR spectra were recorded in DMSO-d_6 solution, the assignments of resonances were based on literature data[20] and are in good agreement with the proposed structures (Figs. S1–3). For the ligand, the numbering of protons used for ^{1}H and ^{13}C NMR is shown in Scheme 1 and the proposed structures of the complexes are reported in Scheme 2. The eight proton signals of DTBTA ligand coordinated to Pt(II) ion for **1** and the sixteen proton signals of two molecules of DTBTA coordinated to Pd(II) ions for **2** are shifted downfield compared to the free ligand as reported in literature for similar ligands with transitional metal ions.[20] The protons C_4H and $C_{4'}H$ in the complex **1** are the most shifted, this confirms that the DTBTA behaves as bidentate ligand, coordinating Pt(II) ion via N(3) atoms of benzothiazole. The ^{13}C NMR spectrum for the complex **1** shows the same trend of ^{1}H NMR spectrum in fact the carbons C_2, $C_{2'}$, C_8, $C_{8'}$, C_9 and finally $C_{9'}$, move to lower field compared to the ligand. In the complex **2** the protons C_4H and C_7H are more shifted respect to the ligand and to the complex **1**, this fact could be due to the second moiety of ligand coordinated to the second Pd(II) ion[21,22]. The sharp and high signals in ^{1}H NMR spectra of complexes in DMSO at 24 h and 48 h rule out a ligand substitution and fragmentation by DMSO. The IR spectrum of the free ligand shows three characteristic bands due to stretching vibration ν(C=N), ν(C–N) and ν(C–S) respectively for benzotriazole rings. In the IR spectra of complexes

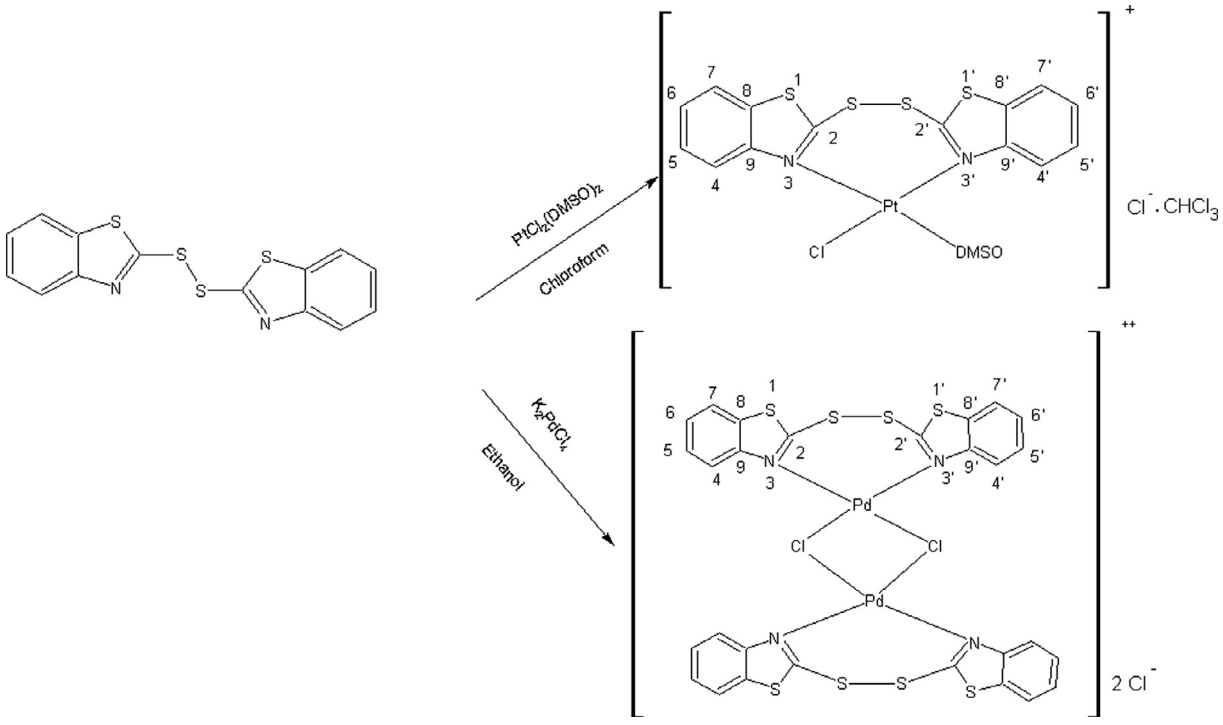

Scheme 2. Procedures of synthesis, structures and numbering scheme of atoms of complexes **1** and **2**.

Table 1
MIC (µM) of complex **1**, complex **2**, DTBTA ligand, tetracycline, cisplatin. NA: not active until 20 µM.

	Complex 1	Complex 2	DTBTA	Tetracycline	Cisplatin
K. rhizophila	2.5	7.5	30	5	5
E. coli	>20	>20	NA	4	5

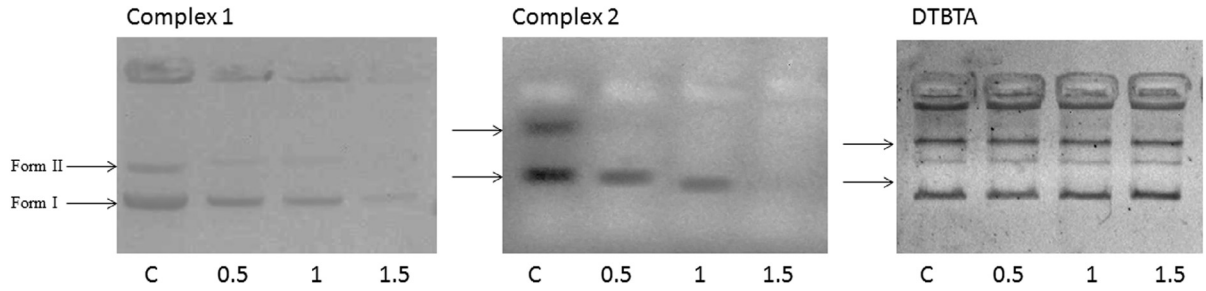

Fig. 1. Gel electrophoresis of plasmid DNA in presence of increasing concentrations (0.5–1.5 mg/ml) of complex **1**, complex **2** and DTBTA. C indicates the plasmid DNA alone. The arrows indicate the two forms of the plasmid, the closed circular (Form I) and the nicked one (Form II).

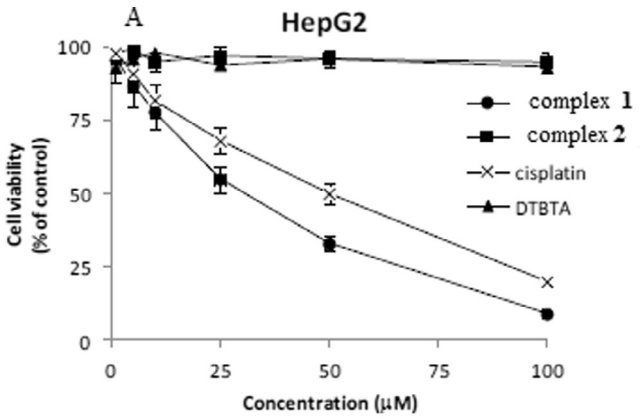

C

	IC50 ± SD (μM)	
	HepG2	MCF-7
complex **1**	20.2±1.8	4.0±0.2
cisplatin	58.0±5.1	7.9±0.6

Fig. 2. Effect of the complex **1**, complex **2** and relative ligand on the viability of HepG2 (**A**) or MCF-7 (**B**) cells. Cells were treated with the compounds and cell survival was measured after 24 h by MTT assay in comparison to cells treated with vehicle alone (control), as reported in *Experimental*. Cisplatin was used as a positive control. Values are the mean ± SD of three separate experiments carried out in triplicate. (**C**) Table shows IC_{50} ± SD values relative to the indicated compounds.

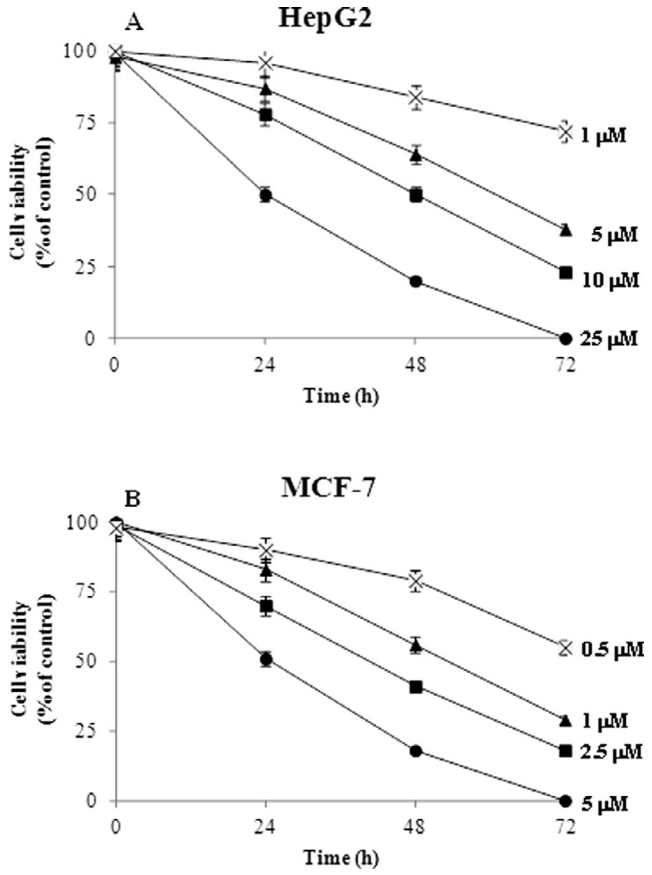

Fig. 3. Inhibitory effect of the complex **1** on the growth of HepG2 (**A**) or MCF-7 (**B**) cells. Cell monolayers were incubated for 24–72 h with complex **1** at the indicated concentrations. Cell viability was assessed by MTT test as reported in *Experimental*. Results are indicated as the percentage of viable cells with respect to untreated controls. Values are the mean ± SD of three separate experiments carried out in triplicate.

1 and **2,** a characteristic band due to *ν*(C=N) vibrations, are shifted after complexation of the ligand to the metal ions.[23] Instead, the band due to *ν*(C–S) vibration of the ligand is unshifted in both complexes, which confirms the coordination on N(3) of the ligand. Moreover, the stretching vibrations of Pt–N and Pd–N bonds for **1** and for **2** are very interesting for the coordination of the ligand to Pt(II) an Pd(II) ions. The presence of *ν*(Pt–Cl) and *ν*(Pd–Cl) bands in the **1** and in **2** complexes, respectively, were due to stretching vibrations of Pt–Cl and *cis*-bridging chloride bonds to Pd(II) ion.[24] In the complex **1** a molecule of DMSO is confirmed by two signals of double S–O and Pt–S bonds.[25,26]

3.2. Biological activity

3.2.1. Antimicrobial activity

Antimicrobial assays of the complexes **1** and **2** against *K. rhizophila* and *E. coli* showed that both are more active against Gram positive than Gram negative bacteria, complex **1** showed a MIC of 2,5 μM and complex **2** a MIC of 7.5 μM against *K. rhizophila*, respectively, as shown in Table 1. In our tested conditions, 5 μM of tetracycline and cisplatin were able to inhibit *K. rhizophila* growth, respectively, and 2,2′-dithiobis(benzothiazole) was active only against *K. rhizophila* (MIC of 30 μM). Differently, both complexes resulted less active in inhibiting the growth of E. coli with MIC larger than 20 μM. These results demonstrated that complex **1** is more effective than cisplatin in the inhibition of *K. rhizophila*; in both cases complexation with metals improved antibacterial activity of DTBTA. Moreover, complex **1** resulted more active than cisplatin against pathogenic Gram-positive bacteria than against Gram-negative bacteria (data not shown).

3.2.2. DNA binding study by gel electrophoresis

As reported in[2,6,27], benzothiazole, Pt(II) and Pd(II) complexes are known to bind DNA. The binding to the DNA of the plasmid pUC19 was monitored by agarose gel electrophoresis. When electrophoresis is applied to circular plasmid DNA, different forms could be detected, i.e. a more abundant and faster form due to the closed circular conformation (Form I) and a slower-moving nicked conformation (Form II).

Fig. 1 shows the results of incubation of complex **1**, complex **2** and DTBTA with the plasmid pUC19. It has been observed from gel electrophoresis that the DTBTA has no effect on the plasmid DNA, while both complexes induced the disappearance of Form I and II at concentration of 1.5 mg/ml. These results suggest that both complexes can bind pUC19 DNA. This binding is likely to occur through intercalation binding mode thanks to the benzothiazole ligand.

3.2.3. Antitumor activity

Cytotoxicity in vitro of the complex **1** and complex **2** was measured on two tumor human cell lines, HepG2 (hepatocellular carcinoma) and MCF-7 (breast cancer), using cisplatin as a positive control. Monolayer cultures treated for 24 h with 1–100 μM concentrations of the compounds were examined by MTT assay for the cell viability. As shown in Fig. 2 A and B, a clear dose dependent inhibitory effect of the complex **1** on the viability of both the cancer cell lines was measured, whereas complex **2**, as well as the ligand (DTBTA), did not affect the cell viability at any of the considered concentrations. The calculated half maximal inhibitory concentration (IC_{50}) values indicated that cytotoxic efficacy of complex **1** was two times higher than that exerted by cisplatin (Fig. 2 C). Moreover, prolonged incubation times (48–72 h) with

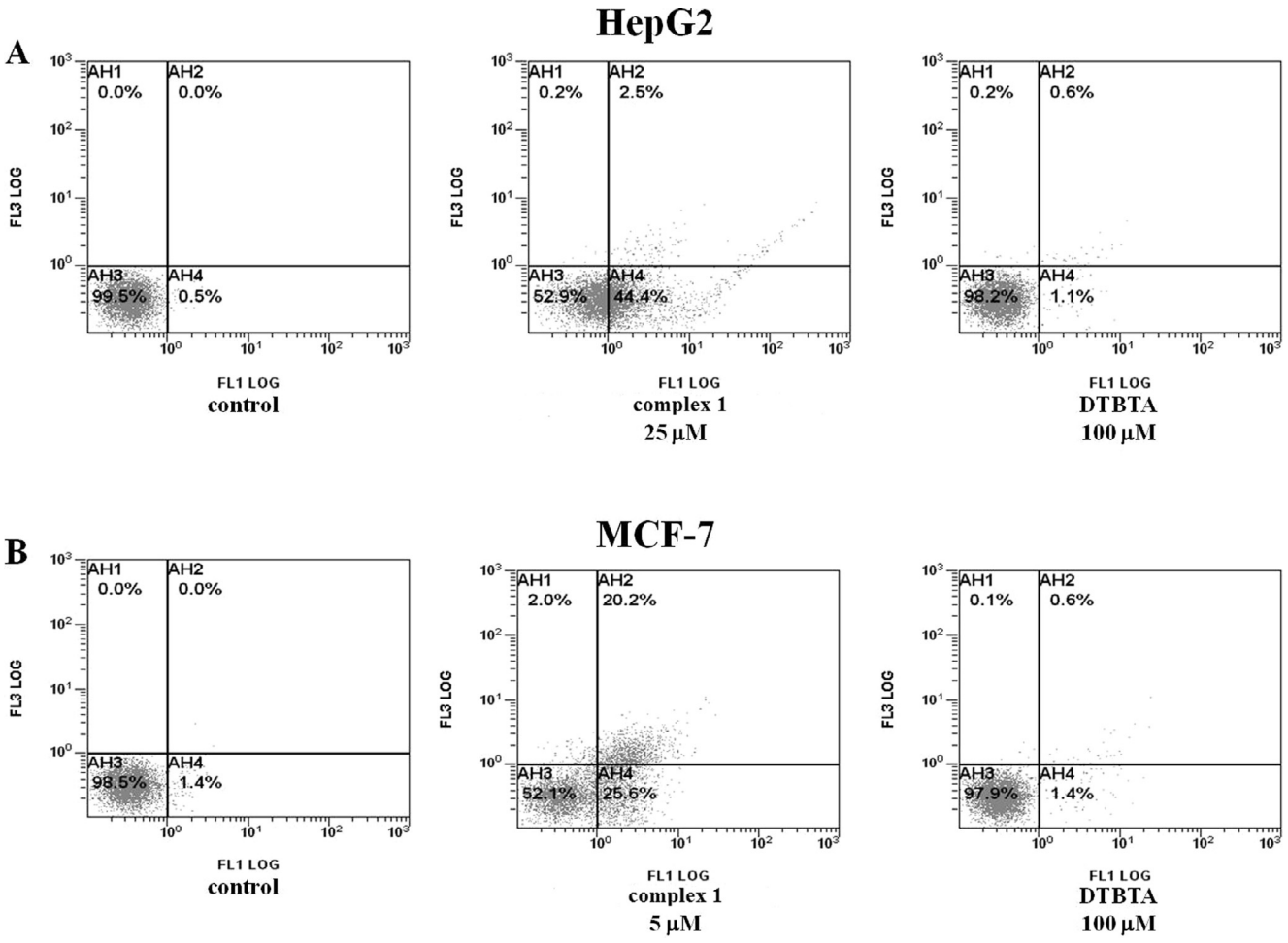

Fig. 4. Flow cytometric analysis for the quantification by AnnexinV/PI double staining of the complex **1** induced apoptosis in HepG2 (**A**) or MCF-7 (**B**) cells. Cell monolayers were incubated for 24 h in the absence (control) or in the presence of the synthesized complex and submitted to double staining with Annexin V/PI as reported in *Experimental*. Ligand was used as negative control. AH3, viable cells (AnnexinV−/PI−); AH4, cells in early apoptosis (AnnexinV+/PI−); AH2, cells in tardive apoptosis (AnnexinV+/PI+); AH1, necrotic cells (AnnexinV−/PI+). Representative images of three experiments with comparable results.

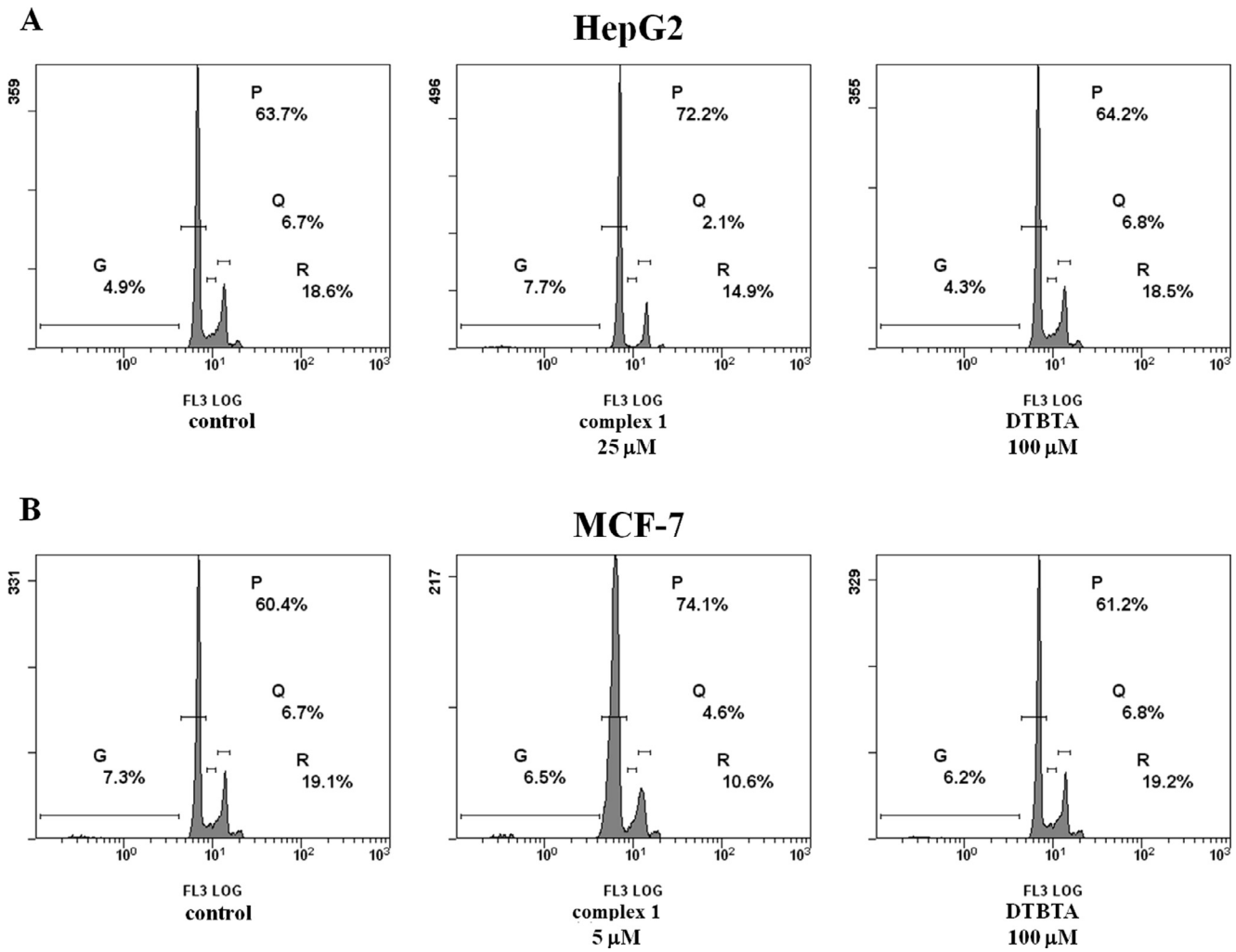

Fig. 5. Effect of complex **1** on the cell cycle distribution of HepG2 (**A**) or MCF-7 (**B**) cells. Flow cytometric analysis of propidium iodide-stained cells after 12 h treatment in the absence (control) or in the presence of the synthesized complex . Ligand was used as negative control. The percentage of cells in the different phases of the cycle was calculated by Expo32 software. Representative images of three experiments with comparable results.

complex **1** resulted in a progressive cell growth inhibition, demonstrating antiproliferative activity of the compound (Fig. 3). Mechanism of the complex **1** induced cell death (necrosis or apoptosis) was investigated both on HepG2 and MCF-7 cells by double staining with propidium iodide (PI) and Annexin V-FITC followed by cytofluorimetric analysis. The chosen concentrations were selected on the basis that they represented the IC_{50} values measured at 24 h for each cell line. As shown in Fig. 4 the complex **1** induced a clear shift of viable cells towards early apoptosis in HepG2 or towards late apoptosis in MCF-7 cells, while did not exert necrotic effects in any cancer cell line. Cells treated with DTBTA at 100 µM, as a negative control, showed a dot plot quite similar to the control cells. Moreover, to determine alterations in the cell cycle caused by the complex **1**, flow cytometry analysis of nuclear DNA content after 12 h treatment of HepG2 and MCF7 cells was carried out. Compared to control cells, complex **1** caused, in both the cancer cell lines, an accumulation of cells in G0/G1phase, paralleled by a reduction in the percentage of cells in the S and G2/M phases (Fig. 5).

To confirm apoptotic mechanism of cytotoxicity of the studied complex **1**, we carried out morphological evaluation of the HepG2 and MCF-7 tumor cells using AO and EB fluorescent DNA binding dyes. The fluorescent microscopy revealed that the nucleus of the control cells was round and the cells stained green, indicating they were normal (Fig. 6). Treatment with **1** for 24 h at IC_{50} concentration caused changes to cell morphology of both tumor lines, with the appearance of cells containing bright green patches in the nuclei as a consequence of chromatin condensation and nuclear fragmentation, which are typical features of apoptosis (Fig. 6). Moreover, fluorescing orange cells owing to increase of cell permeability to ethidium bromide, cell shrinkage and membrane blubbing were also evident as cells in late apoptosis, chiefly in MCF-7 cell line (Fig. 6 B). In order to better understand the cytotoxic activity of the new complexes of platinum and palladium, we have determined cellular platinum uptake on MCF-7 and HepG2 cells after 24 h continuous exposure with 25 µM or 100 µM concentration compounds. The amount of intracellular platinum, evaluated for complex **1** gave a value of $9.5 \cdot 10^{-4}$ ng/cell on MCF-7 and $8.2 \cdot 10^{-4}$ ng/cell on HepG2 cells respectively and the absence of intracellular palladium for complex **2**.

4. Conclusion

Two new mono-Pt(II) and binuclear chloro-bridged Pd(II) complexes with DTBTA ligand were synthesized and characterized. Different structures for **1** and **2** complexes were found; in the complex **1**, the coordination of Pt(II) ion involves the N(3) atoms of the

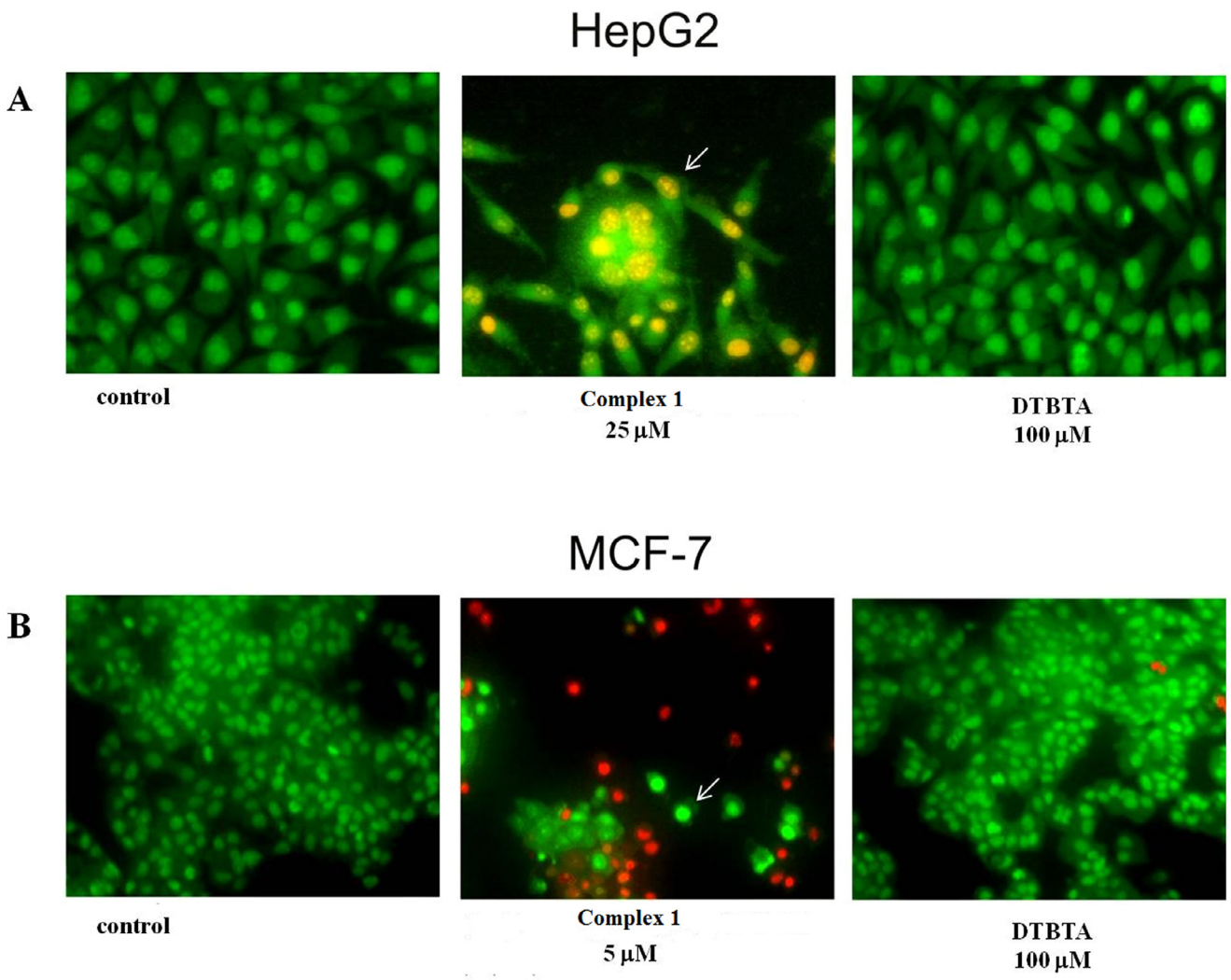

Fig. 6. Fluorescence micrographs of EB/AO double stained HepG2 (**A**), MCF-7 (**B**) cells after treatment with complex **1.** Cells were incubated for 24 h in the absence (control) or in the presence of the synthesized complex and submitted to double staining with AO/EB as reported in *Experimental.* Ligand was used as negative control. Arrows indicate membrane blubbing. Representative images of three experiments with comparable results (200× magnifications).

ligand that acts in a bidentate mode. In binuclear complex **2**, two Pd(II) ions are linked to two molecules of the ligand through chloro-bridged atoms. The geometry of the complexes is square planar, but the structures of **1** and **2** are very different, the second compound is a steric hindered complex. The different structures reflect a different behavior in the antimicrobial and in the antitumor activity. In fact, only **1** shows a dose-dependent anti-proliferative effect against the two tumor cell lines associated to cell apoptosis, while both **1** and **2** exhibit antimicrobial activity with complex **1** more active against Gram positive bacterial growth than cisplatin. The low activity against Gram negative bacteria could be due to the presence of an additional outer membrane in this group of bacteria that could hinder the uptake of both compounds.

Complex **1** is effective inducer of apoptotic death on HepG2 and MCF-7 cells and causes cell arrest at G0/G1 phase. Apoptosis effect is associated with externalization of plasma membrane phosphatidylserine, chromatin condensation, nuclear fragmentation and membrane blubbing. Complex **2** is ineffective, indicating that only the coordination with Pt(II) ion confers to DTBTA potential pharmacological properties. Both complexes were found to bind DNA, and we can surmise that the binding is due to intercalation binding mode thanks to the benzothiazole ligand. The different behavior of the two complexes depends upon the different uptake, indeed uptake study demonstrated only the presence of intracellular platinum in HepG2 and MCF-7 cells, suggesting that the Pd(II) complex cannot enter into the cells likely for its dimeric structure.

Acknowledgements

Financial support by the Ministero dell'Istruzione, dell'Università e della Ricerca, Rome and by the University of Palermo is gratefully acknowledged. We are grateful to Diana Amorello (University of Palermo, STEBICEF Department) for the significant contribution in Voltammetry measurements.

A. Supplementary data

Supplementary data associated with this article can be found, in the online version, at http://dx.doi.org/10.1016/j.bmc.2017.02.067.

References

1. Akhtar J, Khan AA, Ali Z, Haider R, Shahar Yar M. *Eur J Med Chem*. 2017 (in press).
2. Keri RS, Patil MR, Patil SA, Budagumpi SS. *Eur J Med Chem*. 2015;89:207–251.
3. Zablotskaya A, Segal I, Geronikaki A, et al. *Eur J Med Chem*. 2013;70:846–856.
4. Singh MK, Tilak R, Nath G, Awasthi SK, Agarwal A. *Eur J Med Chem*. 2013;63:635–644.
5. Abdel Ghani NT, Mansour AM. *J Mol Struct*. 2011;991:108–126.
6. Gao EJ, Wang KH, Gu XF, et al. *J Inorg Biochem*. 2007;101:1404–1409.

7. Fanelli M, Formica M, Fusi V, Giorgi L, Micheloni M, Paoli P. *Coord Chem Rev*. 2016;310:41–79.
8. Alam MN, Huq F. *Coord Chem Rev*. 2016;316:36–67.
9. Rubino S, Portanova P, Girasolo A, Calvaruso G, Orecchio S, Stocco GC. *Eur J Med Chem*. 2009;44:1041–1048.
10. Rubino S, Portanova P, Giammalva F, et al. *Inorg Chim Acta*. 2011;370:207–214.
11. Farrell N, Kelland LR. In: Farrell NP, ed. *Platinum-Based Drug in Cancer Therapy*. Totowa: Humana Press; 2000:321–338.
12. Schőniger W. *Mikrochim Acta*. 1955;123–129.
13. Price JH, Williamson AN, Schramm RS, Wayland BB. *Inorg Chem*. 1972;11:1280–1284.
14. Geary WJ. *Coord Chem Rev*. 1971;7:81–122.
15. Giardina A, Alduina R, Gottardi E, Di Caro V, Süssmuth RD, Puglia AM. *Microb Cell Fact*. 2010;9:44.
16. Lo Grasso L, Maffioli S, Sosio M, Bibb M, Puglia AM, Alduina R. *J Bacteriol*. 2015;197:2536–2544.
17. Randazzo L, Montana G, Alduina R, Quatrini P, Tsantini E, Salemi B. *J Cult Herit*. 2015;16:838–847.
18. Vitale M, Scatassa ML, Cardamone C, et al. *Foodborne Pathog Dis*. 2015;12:21–23.
19. Alduina R, Lo Piccolo L, D'Alia D, et al. *J Bacteriol*. 2007;189:8120–8129.
20. Valdés H, Reyes-Martínez R, Pioquinto-Mendoza JR, et al. *Inorg Chim Acta*. 2015;431:222–229.
21. Chaudhari KR, Wadawale AP, Jain VK. *J Organomet Chem*. 2012;698:15–21.
22. Handerson JK. Organometallic and homogeneous catalytic chemistry of palladium and platinum. In: Hartley FR, ed. *Studies in inorganic chemistry. Chemistry of the platinum Group Metals*, 11. Amsterdam-Oxford-New York-Tokyo: Elsevier; 1991.
23. Rubino S, Pibiri I, Costantino C, et al. *J Inorg Biochem*. 2016;155:92–100.
24. Nakamoto K. *Infrared and Raman Spectra of Inorganic and Coordination Compounds, Part B: Applications in Coordination, Organometallic and Bioinorganic Chemistry*. 5th Ed. U.S.A.: A Wiley-Interscience Publ.; 1997.
25. Rubino S, Di Stefano V, Attanzio A, et al. *Inorg Chim Acta*. 2014;418:112–118.
26. Dodoff NI, Kovala-Demertzi D, Kubiak M, Kuduk-Jaworska J, Kochel A, Gorneva GA. *Z Naturforschung*. 2006;61b:111–1121.
27. Sharma K, Singh RV, Fahmi N. *Spectrochimica Acta Part A*. 2011;78:80–87.